Geochimica et Cosmochimica Acta, Vol. 69, No. 19, pp. 4649–4664, 2005

0016-7037/05 $30.00 + .00

ELSEVIER

doi:10.1016/j.gca.2005.05.019

Effects of *in situ* remediation on the speciation and bioavailability of zinc in a smelter contaminated soil

M. NACHTEGAAL,[1,*] M. A. MARCUS,[2] J. E. SONKE,[3] J. VANGRONSVELD,[4] K. J. T. LIVI,[5] D. VAN DER LELIE,[6] and D. L. SPARKS[1]

[1]Department of Plant and Soil Sciences, University of Delaware, 152 Townsend Hall, Newark, DE 19717-1303, USA
[2]Advanced Light Source, Lawrence Berkeley National Laboratory, One Cyclotron Road, Berkeley, CA 94720, USA
[3]National High Magnetic Field Laboratory, Geochemistry Division, 1800 E. Paul Dirac Dr., Tallahassee, FL 32306, USA
[4]Limburgs Universitair Centrum, Environmental Biology, Universitaire Campus, B-3590 Diepenbeek, Belgium
[5]Department of Earth and Planetary Sciences, Johns Hopkins University, 34th and North Charles Streets, Baltimore, MD 21218, USA
[6]Biology Department, 463 Brookhaven National Laboratory, Upton, NY 11973-5000, USA

(*Received January* 11, 2005; *accepted in revised form May* 26, 2005)

Abstract—We report results from an extensive study on the speciation of zinc (Zn) and its relation to the mobility and bioavailablity of this element in a smelter contaminated soil and an *in situ* remediated area of this soil 12 yr after the application of cyclonic ash and compost. Emphasis was placed on the role of neoformed precipitates in controlling Zn speciation, mobility and bioavailability under different environmental conditions. Twelve years after remediation, the pH of the treated and non-treated soil differed by only 0.5 pH unit. Using state-of-the-art electron and X-ray microscopies in combination with micro-focused extended X-ray absorption fine structure (μ-EXAFS) spectroscopy, no major differences in Zn speciation were found between samples of the treated and non-treated soil. In both soils, 30% to 50% of Zn was present in smelter related minerals (willemite, hemimorphite or gahnite), while 50% to 70% of Zn was incorporated into newly formed Zn precipitates. Contrary to the non-treated soil, the treated soil did not contain gahnite or sphalerite; it is possible that these minerals were dissolved under the higher pH conditions at the time of treatment. Desorption experiments, using a stirred flow technique with a 0.1 mol/L $CaCl_2$ (pH 6.5) and a HNO_3 (pH 4.0) solution were employed to determine the exchangeable Zn fraction and the Zn fraction which will be mobilized under more extreme weathering conditions, respectively. No significant differences were found in desorption behavior between the treated vs. non-treated soil. Bioavailability tests, using the *R. metallidurans* AE1433 biosensor showed that ~8% of total Zn was bioavailable in both the treated and non-treated soils. It was concluded that the incorporation of Zn into newly formed precipitates in both the treated and non treated soils leads to a significant natural attenuation of the exchangeable/bioavailable Zn fraction at near neutral pH conditions. At lower pHs, conditions not favorable to the formation of Zn precipitates, the pool of Zn associated with the secondary Zn precipitates is potentially more bioavailable.

1. INTRODUCTION

Elevated concentrations of non-ferrous metals (Zn, Cd, Pb, etc.) and their toxic effects to local ecosystems have been frequently documented in surface soils near base metal smelters. In some cases these high metal concentrations have led to a complete destruction of the natural vegetative cover (Vangronsveld et al., 1996). In a 1983 survey of worldwide trace element emissions, the Zn flux into the atmosphere from Zn production using the highly polluting pyrometallurgical smelting process was estimated at 50% to 70% of the total atmospheric Zn flux (Nriagu and Pacyna, 1988). Today, most Zn is extracted from the ore by a hydro-metallurgical process. However, the pyrometallurgical smelting process has been used for over two centuries and produced highly contaminated sites all over the world (Wickham, 1990).

In situ remediation (immobilization/inactivation) of vast contaminated sites using soil amendments, which modify the physicochemical properties of the contaminating heavy metals, is a valuable alternative to more expensive and complicated civil-engineering techniques, e.g. excavation and landfilling of contaminated soil (Vangronsveld et al., 1996). Many additives have been screened for their potential to immobilize heavy metals in soils. Examples of these additives include lime (Mench et al., 1994a; Sparks, 1995), zeolites (Gworek, 1992a, 1992b; Chlopecka and Adriano, 1997; Rebedea and Lepp, 1994; Oste et al., 2002), ashes from fluidized bed burning of coal mine waste (Vangronsveld et al., 1995, 1996), phosphates and apatites (Ma et al., 1993, 1995; Laperche et al., 1996; Ma, 1996; Chlopecka and Adriano, 1997; Boisson et al., 1999), iron and manganese oxide bearing materials (Mench et al., 1994a, 1994b), and red mud (Krebs-Hartmann, 1997; Lombi et al., 2003). Each of these additives has a different effect on bioavailability of the metals, micronutrient availability, soil solution pH and soil microstructure (Mench et al., 1998; Lombi et al., 2003; Oste et al., 2002).

Regulatory acceptance of *in situ* immobilization as an effective reclamation method depends on the ability to predict the long-term stability of such remedial treatments. In order to realistically address the long term stability of the metals, one needs to probe metal (e.g. Zn) speciation changes as a result of the soil reclamation activities and determine if these changes in the metal speciation have lead to a sequestration of the metal over the course of its residence time.

Traditionally, metal speciation in soils has been determined

* Author to whom correspondence should be addressed (maarten.nachtegaal@psi.ch).
Present address: Paul Scherrer Institute, Swiss Light Source, Office: WGLA/219, CH-5232 Villigen PSI, Switzerland

using sequential selective extractions, which are widely applied. The purpose of sequential extractions is to provide detailed information on metal origin, biological and physicochemical availability, mobilization, and transport (Tessier et al., 1979). This approach to metal speciation describes soil as having several fractions with which metals can be associated, such that these fractions can be attacked by chemicals specific to each fraction (Roberts et al., 2005). The use of sequential extractions for metal speciation is not without its limitations and pitfalls. These include (1) the incomplete dissolution of target phases, (2) the removal of a non-target species, (3) the incomplete removal of a dissolved species due to re-adsorption on remaining soil components or due to re-precipitation with the added reagent and (4) change in the valence of redox-sensitive elements (Brümmer et al., 1983; Gruebel et al., 1988; Ostergren et al., 1999; La Force and Fendorf, 2000; Calmano et al., 2001; Roberts et al., 2005). These limitations are becoming more evident with the appearance of new literature on sequential extractions coupled with analytical techniques capable of directly determining metal speciation in soils and sediments (Gruebel et al., 1988; Adamo et al., 1996; Henderson et al., 1998; Ostergren et al., 1999; La Force and Fendorf, 2000; Calmano et al., 2001; Scheinost et al., 2002).

Synchrotron based X-ray absorption fine structure (XAFS) spectroscopy is a technique that can provide detailed chemical and structural information about a specific absorbing element *in situ* with minor or no pretreatments (Bertsch and Hunter, 1998). XAFS spectroscopy has become the method of choice for probing the speciation of metal contaminants at the molecular level and its use has demonstrated the variable reactivity and speciation of Zn in model systems. One important conclusion of studies on the complexation mechanisms of Zn with aluminosilicates is that Zn may be incorporated into neoformed precipitates under neutral to basic conditions in the presence of the aluminosilicate surfaces (Ford and Sparks 2000; Schlegel et al., 2001; Trainor et al., 2000). The formation of Zn-containing neoformed precipitates may greatly reduce the bioavailability of Zn in contaminated soils when the pH is raised (Juillot et al., 2003).

The disadvantage of using bulk XAFS to speciate Zn in heterogeneous systems, such as soils, is that it probes a volume of several cubic millimeters, thereby averaging over all the atoms of a given element in the system under study, regardless of their chemical state (Manceau et al., 2002). The short range structural information extracted by non-linear least-square multishell fitting is usually sufficient to determine the dominant species in a sample. However, when Zn is present in multiple phases, the atomic shells from the different species overlap and cannot be distinguished when there is a mixture (Manceau et al., 2002). With the advent of high-brilliance synchrotron radiation sources it is now possible to identify metal species in dilute samples with high spatial resolution, using micro-focused extended X-ray absorption fine structure spectroscopy (μ-EXAFS). When probing only a small area of a sample, typically several square micrometers, one minimizes the number of species contributing to the overall spectrum. By fitting linear combinations of spectra of known Zn-compounds to the unknown raw spectrum, one can then identify the major species contributing to the overall spectrum (Manceau et al., 1996). The success of such a fitting approach depends on the availability of all unknown species in the reference database.

Even when a large database of reference spectra is available and a good fit is achieved, some doubts remain whether a unique solution is achieved (Wasserman et al., 1999). To tackle this problem one could apply principal component analysis (PCA) to the set of spectra, to determine how many independent components are needed to reproduce the complete dataset. Through subsequent target transformation analysis, the real reference spectra which make up the abstract principal components can be identified. The reference spectra identified with PCA can than be used to obtain a more unique linear combination fit. One must realize that equally-good fits can be obtained when references in the database are very similar to each other, in which one reference substitutes for the other. In that case PCA analysis will not distinguish between the similar references (Manceau et al., 2002).

Metal 'bioavailability' can be defined as the fraction of the total metal content of the soil that can interact with a biological target (Geebelen et al., 2003). The bioavailability of a metal can not be automatically correlated to the "exchangeable" Zn fraction, since the metal bioavailability does not only depend on the physical, biological, and chemical characteristics of the medium affected, but also on the metal species and the biological species. To get information on the bioavailability of a specific heavy metal, such as Zn, and not just the general bioavailabiliy, bacterial biosensors (BIOMET) have been developed which detect the presence of a specific heavy metal (Corbisier et al., 1996; Van der Lelie et al., 1997).

The objectives of this study were: (1) to evaluate, based on direct speciation assessments, the impact of long term remediation with a mineral additive and compost on Zn speciation in smelter-affected soils, (2) to relate Zn speciation to Zn bioavailability and mobility and (3) to evaluate the importance of newly formed Zn-precipitates in the reduction of the (bio)available Zn fraction in the smelter contaminated soils.

The samples used in this study were collected from a highly contaminated zinc smelter site in Belgium, where several remediation strategies have been tested and a remediation project has been conducted for $>$ 12 yr (Vangronsveld et al., 1996). Samples were collected from the non-treated area, and from an area 12 yr after treatment with cyclonic ash and compost. Conventional soil chemistry techniques were combined with micro-focused X-ray fluorescence (XRF) and EXAFS spectroscopy to speciate Zn in the treated and non-treated soils. Zinc mobility in the treated and non-treated soils was determined with stirred-flow desorption experiments, using a 0.1 mol/L $CaCl_2$ solution adjusted to the soil pH, and a pH 4 HNO_3 solution to obtain the exchangeable and acid extractable Zn fraction. A Zn microbial sensor (BIOMET) was used to estimate the current Zn bioavailability in the treated and non-treated soils.

2. MATERIALS AND METHODS

2.1. Site Description and Sampling

Soil samples were collected from a former zinc smelter site located near the 'Lommel' smelter in northeastern Belgium (for a map of the area, see Vangronsveld et al., 1996). Due to the high concentrations of different non-ferrous metals in the soil, a vegetative cover was lacking over 135 ha in 1990. In 1990, 3 ha of this area were successfully

revegetated by the *in-situ* immobilization of toxic metals through a mineral additive and the subsequent planting of metal tolerant plants (Vangronsveld et al., 1995). The mineral additive used was cyclonic ash (a modified aluminosilicate produced by burning coal refuse in a fluidized bed) together with organic compost. Since 1998, an increasing colonization could also be observed of the non-treated area by metal-tolerant plants from the treated area. Samples were collected from the upper 20 cm of the bare contaminated area (henceforth called 'non-treated') and from the upper 20 cm of the remediated site (called 'treated'), 12 yrs after the soil treatment. Two kilograms of soil were collected randomly from each area and homogeneously mixed before analysis. The samples were dried at 80°C and passed through a 2-mm sieve.

2.2. Bulk Soil Parameters

The pH of the treated and non-treated samples was determined by mixing a 0.01 mol/L $CaCl_2$ solution with the soil in a 10:1 weight ratio, equilibrating for 2 h and subsequently measuring the pH. Dry weight Pb, Zn, Cu, Cd, As, Ni, Co, Fe, Mn, P, S, Ba, Al, Ti and Zr concentrations and Pb isotope ratios were measured on a Finnigan ELEMENT 1, high resolution magnetic sector inductively coupled plasma mass spectrometer (HR-ICP-MS) at the National High Magnetic Field Laboratory (Tallahassee, USA). All sample handling was conducted in a class 100 clean lab and flow bench. One hundred milligrams (100 mg) of soil was digested at 125°C for 16 h, in an ultra pure acid mixture, consisting of 3 mL HF (double distilled), 4 mL HNO_3 (double distilled) and 3 mL $HClO_4$ (SEASTAR Chemicals Inc.). Digests were dried at 175°C, taken up in 2 mL of 6 N HNO_3 and diluted to 100 mL total volume in pre-cleaned HDPE bottles. For HR-ICP-MS analyses, samples were diluted 100-fold with 0.17 N HNO_3, such that the total dissolved solid fraction was 10 ppm. Triplicate samples and procedural blanks were analyzed against a mixture of known standards (High Purity Standards). All samples, blanks and standards were spiked with Sc, In and Tl to track instrument drift and potential matrix effects. The external reproducibility for the triplicate samples was $> 10\%$ for most elements.

For Pb isotope ratio measurements, an external fractionation correction was applied by alternatively measuring NBS981 and the samples in the 10ppm total dissolved sample dilution. Pb isotopes were measured in low resolution with an analogue detection mode. Reproducibility based on in-run replicates of NBS981 ($n = 5$) was $> 0.05\%$ for all ratios.

2.3. Stirred-Flow Desorption

Desorption experiments were conducted using two different desorptive solutions: (1) a 0.1 mol/L $CaCl_2$ solution adjusted to the soil pH (6.5), and (2) a HNO_3 (pH 4) solution. A stirred-flow technique was used for the desorption experiments. The small sample chamber, relatively low solid: solution ratio and constant flow rate ensured that none of the desorption products would be re-adsorbed onto the soil. The experimental setup for the Zn desorption studies was similar to that illustrated by Strawn and Sparks (2000). Briefly, a stirred-flow reaction chamber was connected to an HPLC pump at the inlet and to a fraction collector at the outlet. The desorptive solution was pumped through the chamber at a flow rate of 0.8 mL min^{-1}. The chamber was covered with a 25-mm filter membrane of 0.2-μm pore size to separate the solids from the solution. The chamber volume of ~8 mL contained a suspension of 0.3 g of soil, which was stirred at 400 rpm with a magnetic stir bar. Effluent aliquots of 10 mL were sampled at the chamber outlet and analyzed for Zn by inductively coupled plasma optical emission spectrometry (ICP-OES). The data from the stirred-flow studies were plotted as a function of chamber volumes (CV), which were calculated by multiplying the flow rate by the time and dividing by the volume of the chamber (8 mL; $CV = ([mL \times min^{-1}] \times [min])/[ml^{-1}]$.

2.4. Bioavailability Test

Bacterial availability of Zn was assessed using a bacterial biosensor strain *Ralstonia metallidurans* (formally called *Alcaligenes eutrophus*) AE1433. This strain contains a fusion between the cadmium, zinc and cobalt resistance operon (Nies et al., 1989; van der Lelie et al., 1997) and the lux reporter system. This test strain has light production as detectable signal (BIOMET; Corbisier et al., 1996) and reacts specifically in the presence of bioavailable Zn. The soil samples, standard, and blank assays were analyzed using a Luminescan (Labsystems) luminometer at 23°C as described before (Corbisier et al., 1999). Soil suspensions were prepared by diluting 5 g of soil with 30 g of reconstitution media. The soil suspensions were then diluted 2, 4, 8, 16 and 32 times and finally added in duplicate to a 96-well microtiter plate, which contained the AE1433 biosensor culture. The light production of the biosensor was monitored over a 12-h period every 30 min.

The induction of bioluminescence (presented as the signal to background (S/B) ratio) is calculated as the light production value (S) found for the samples tested, divided by the light production value found for an uncontaminated control soil (background, B), containing similar physical-chemical characteristics (pH, CEC, texture, organic matter, nutrient status). The control soil was sampled in the north east of Belgium away from the zinc smelter. An induction is considered as significant when a S/B ratio of at least 2 is found. With a calibration curve set up for Zn, these ratios allow one to calculate the amount of bioavailable Zn (mg Zn eq. kg^{-1} soil) (Corbisier et al., 1999; van der Lelie et al., 1999). As a control, the bacterial strain AE864, which shows constitutive light production, was used to monitor toxicity which could bias the interpretation of the metal bioavailability test. In the absence of toxicity or matrix effects that influence bioluminescence, strain AE864 will show a S/B ratio of 1. The Zn bioavailability data collected with strain AE1433 were only considered as valid when at the same time strain AE864 showed a S/B ratio between 0.8 and 1.2.

2.5. Electron Probe Microanalysis (EPMA)

Electron microprobe analysis was performed using a JEOL JXA-8600 microprobe (John Hopkins University) equipped with both wavelength-dispersive and energy-dispersive spectrometers (WDS and EDS). Two sub samples of the treated and the non-treated samples were embedded in Scotchdale Resin, mounted on pure quartz slides, polished to 30-μm thin sections, and sputter coated with carbon before microprobe analysis. Samples were scanned manually at magnifications of 85× to 300× using backscatter electron imaging to identify heavy metal rich particles. Particles of interest were identified by EDS screening. At selected, representative spots, several elements, i.e. Zn, Pb, Si, Al, S, Mn and Ca, were mapped with EDS and Fe with WDS.

2.6. Preparation, Collection and Analysis of EXAFS Reference Spectra

A large library of natural and synthetic Zn minerals and Zn sorption samples was generated to aid in the spectral analysis of the unknown soil spectra. Franklinite ($ZnFe_2O_4$), willemite (Zn_2SiO_4), hydrozincite ($Zn_5(OH)_6[CO_3]_2$), zincite (ZnO), smithsonite ($ZnCO_3$), and gahnite ($ZnAl_2O_4$) were provided by the Museum of Natural History, Washington, DC. Sphalerite (ZnS) was obtained from Aldrich (spectrum provided by Dr. A. Voegelin) and hemimorphite ($Zn_4Si_2O_7[OH]_2 \cdot H_2O$) was obtained from Excalibur, Peekskill NY.

A Zn-Al layered double hydroxide, a Zn-kerolite ($Zn_3Si4O_{10}[OH]_2 \cdot H_2O$, EXAFS spectrum provided by Dr. A. Manceau) and an amorphous Zn hydroxide were synthesized following published methods (Ford and Sparks, 2000; Schlegel et al., 2001; Waychunas et al., 2002). Sorption samples were prepared by reacting Zn with ferrihydrite (2-line, freshly precipitated) (Schwertmann and Cornell, 1991), goethite (ferrihydrite aged for 3 weeks at 25°C and washed with 0.4 mol/L HCl, 66 $m^2\ g^{-1}$), low-surface area gibbsite (synthesized and aged 30 d, 90 $m^2\ g^{-1}$), birnessite (45 $m^2\ g^{-1}$) (McKenzie, 1971), kaolinite (University of Missouri Source Clays Repository, KGa-1, cleaned, 14 $m^2\ g^{-1}$), hydroxy-Al interlayered montmorillonite (Al reacted SWy-1 [University of Missouri Source Clays Repository, 90 $m^2\ g^{-1}$]), orthophosphate (Aldrich) and humic acid (Aldrich, 99% purity). All sorption samples were prepared in a N_2 atmosphere glovebox using ACS reagent grade chemicals and CO_2-free double deionized H_2O. A 0.1 mol/L $Zn(NO_3)_2$ stock solution was slowly added to suspensions of 10 g/L solids at an ionic strength of 0.1 mol/L $NaNO_3$. Zinc was sorbed to goethite and kaolinite at pH 5, to create inner-sphere sorption complexes and to kaolinite at pH 7 to create a surface induced precipitate, either LDH or

phyllosilicate in character (Nachtegaal and Sparks, 2004). Solids were separated by centrifugation and stored in a refrigerator as wet pastes until EXAFS analyses. All other spectra of sorption spectra were obtained from Dr. D.R. Roberts; for further sample details see Roberts et al. (2002).

Zn K-edge EXAFS spectra of the treated and the non-treated soil samples and Zn powder reference compounds were collected at beamline X-11A at the National Synchrotron Light Source (NSLS), Upton NY. The electron storage ring operated at 2.5 GeV yielding an electron beam of 300 to 100 mA. The double crystal Si(111) monochromator was detuned by reducing I_0 by 30%. The beam energy was calibrated by assigning the first inflection on the K-absorption edge of a Zn metal foil to 9659 eV. All samples were mounted into Teflon sample holders, sealed with Kapton tape, and measured at room temperature in fluorescence mode using a 13-element solid state detector. Depending on the Zn concentration, multiple scans were collected until satisfactory signal-to-noise ratios were achieved. Two sheets of Al foil were used to suppress Fe and to a lesser extent Cu fluorescence from the sample.

EXAFS data reduction of the reference phases was performed using WinXAS 2.1 (Ressler, 1997) following standard procedures (Eick and Fendorf, 1998; Nachtegaal and Sparks, 2003). The χ function was extracted from the raw data by fitting a linear function to the pre-edge region and a spline function to the post-edge region, and normalizing the edge jump to unity. The energy axis (eV) was converted to photoelectron wave vector units ($Å^{-1}$) by assigning the origin, E_0, to the first inflexion point of the absorption edge. The resulting $\chi(k)$ functions were weighted with k^3 (k is the photoelectron wavenumber) to compensate for the dampening of the XAFS amplitude with increasing k and were Fourier-transformed to obtain radial structure functions (RSF). A Bessel window with a smoothing parameter of 4 was used to decrease the amplitude of FT side lobes, due to the finite Fourier filtering range between $\Delta k = 1.5$ and 12 $Å^{-1}$. The two major peaks below 3.5 Å in the Fourier transformed curves were isolated and back-transformed. The back-transformed peaks were individually fit in k space. *Ab initio* Zn-O, Zn-S, Zn-Fe, Zn-Mn, Zn-Al, Zn-C and Zn-Zn scattering paths were generated using the FEFF 7 code (Zabinsky et al., 1995) from the refinement of the structure of lizardite ($Mg_3Si_2O_5[OH]_4$), where Zn, Fe or Mn was substituted for Mg in octahedral positions, and from the structures of franklinite, willemite, smithsonite and zincite. After each of the individual peaks in the Fourier transform spectra were back-transformed and fit, multishell fitting was done in k space over the entire k-range ($\Delta k = 2.1$–10.8) using the same parameters. The E_0 shifts were constrained to be equal for all paths and the Debye Waller factors were constrained to be equal for the metals in the second shell only when two metals were present in the second shell. The amplitude reduction factor, $(S_0)^2$, was fixed at 0.85.

The bond distances (R) were estimated to be accurate to $R \pm 0.02$ Å and $R \pm 0.05$ Å, for the first and second shells, respectively, and coordination numbers (CN) were accurate to $N \pm 20\%$ and $N \pm 40\%$ for the first and second shells, respectively (Roberts et al., 2002). Error estimates were determined by a comparison of XRD and EXAFS results for franklinite and sphalerite, in agreement with estimates previously published (Scheidegger et al., 1997; O'Day et al., 1998).

2.7. Micro-SXRF and μ-EXAFS Data Collection

Micro-focused synchrotron based X-ray fluorescence (μ-SXRF) and Zn-K-edge μ-EXAFS on two resin embedded thin sections of the treated and two of the non-treated smelter soils were performed on beamline 10.3.2 of the Advanced Light Source (ALS), Lawrence Berkeley National Lab, Berkeley, USA (Marcus et al., 2004). The beam was focused down to 16×7 μm for course mapping or 5×5 μm for fine mapping and μ-EXAFS. The monochromater position was calibrated with a Zn metal foil. Soil thin sections were placed at an angle of 45° to the incident beam. Fluorescence X-ray yield was measured at room temperature with a Ge solid-state detector. μ-SXRF maps were collected at 10 keV and with 20-μm steps for large overview maps and 5 m steps for detailed maps. The fluorescence yield was normalized to I_0 and the dwell time. μ-EXAFS spectra were collected on selected representative regions in the thin sections, based on elemental associations obtained from μ-SXRF mapping and optical images from the thin sections.

2.8. Micro Focused-EXAFS Analyses

EXAFS data reduction of the micro focused-EXAFS spectra was performed using the Labview software at beamline 10.3.2 at the ALS. The k^3-weighted χ spectra of the non-treated and treated soil samples were analyzed using principal component analysis (PCA) (Malinowski, 1991; Manceau et al., 2002; Ressler et al., 2002) over the k-range 2.7 to 10.0 $Å^{-1}$. The number of primary components was evaluated using two criteria; the weight of each component, which is directly related to how much of the signal it represents and the indicator (IND) of each component, which reaches a minimum for the least significant component representing a real signal (Malinowski, 1991; Manceau et al., 2002). This IND value is an empirical function and works well in determining the amount of principal components present. The number of principal components found with PCA corresponds to the number of Zn species present in the set of spectra, provided no species has a constant fractional background (Manceau et al., 2002). A target transformation was performed to identify the real references which might make up the abstract principal components. A criterion for determining whether the target transformed candidate resembles the original reference spectrum is given by the SPOIL value (Malinowski, 1978; Manceau et al., 2002). SPOIL measures the degree to which replacing an abstract component with the reference would increase the fit error. This is a non-negative dimensionless number for which values of 1.5 are considered excellent, 1.5 to 3 are good, 3 to 4.5 are fair, 3.5 to 6 are poor and > 6 are unacceptable.

Linear combinations of the references identified by the target transformations as likely components were optimized to fit the k^3-weighted χ μ-EXAFS spectra, with only the fractions of each reference spectrum as adjustable parameters. Fits were optimized by minimizing the normalized sum-square ($NSS = (\{k^3\chi[k]_{exp} - k^3\chi[k]_{reconstr.}\}^2 / (\{k^3\chi[k]_{exp}{}^2)$ (Manceau et al., 2002). A component was only added to the fit if the NSS improved by 20% or more. The accuracy of the fitting approach is dependent on the data quality, range of fitting, and how well the standards represent the unknown sample. The uncertainty in the proportion of individual Zn species was determined to be ~10%, using a similar fitting approach (Isaure et al., 2002).

3. RESULTS

3.1. Bulk Soil Characteristics

Twelve years after remediation of the smelter contaminated area, the pH of the treated site (which was between 7.3 and 7.9 at the time of treatment; Vangronsveld et al., 1995) had reverted back to the pH of the non-treated area, which was ~6.5 (pH values are tabulated in Table 1). Concentrations of elements and isotope ratios for $^{206}Pb/^{207}Pb$ and $^{208}Pb/^{206}Pb$ of the treated and non-treated areas are reported in Table 1 as averages of triplicate analyses. Both the treated and non-treated soil samples contained elevated concentrations of toxic metals. The difference in metal concentrations between the treated and non-treated samples is not related to the treatment with cyclonic ashes and compost, but more likely reflects the *in situ* variation in pollutant concentrations, which had been found in a former study to range from ~2000 to 18,550 mg/kg Zn at the smelter site (Vangronsveld et al., 1996).

Pb isotope ratios between treated and non-treated samples were not significantly different. A comparison of the $^{206}Pb/^{207}Pb$ and $^{208}Pb/^{206}Pb$ ratios of the treated and non-treated soils with a historic Pb isotope record of atmospheric dust deposition at the site (Sonke et al., 2002) indicated that the ratios of the treated and non-treated soils are similar to recent Pb deposition (1960–1990, $^{206}Pb/^{207}Pb$: 1.133 ± 0.001 and $^{208}Pb/^{206}Pb$: 2.125 ± 0.002). This period reflects the last 15 yr (1960–1974) of maximal production and pollution before the smelter was dismantled. Thus, most metals were introduced to the soil > 30

Table 1. pH, metal concentrations and Pb isotope ratios for non-treated and treated soils.

Element	Non-treated (pH = 6.4) (ppm)	Treated (pH = 6.7) (ppm)
Fe	47,880	21,159
Al	18,619	23,264
Ti	1533	1765
Zr	170	175
Ba	513	368
Mn	1122	573
P	357	819
S	2351	1881
Zn	20,476	13,144
Pb	2996	1297
Cu	2132	762
As	312	115
Ni	348	165
Co	41	25
Cd	31	51
Hg	737	779
Hg	737	779
Pb206/Pb207	1.1326	1.1321
	0.0007	0.0007
Pb208/Pb206	2.1296	2.1298
	0.0014	0.0019

yr ago, with the majority of the metals introduced between 30 and 45 yr ago.

3.2. Stirred-Flow Desorption Experiments

In order to assess the exchangeable metal fraction and the metal fraction which is not stable at lower pH, stirred-flow desorption experiments were conducted using a 0.1 mol/L $CaCl_2$ (pH 6.5) or a HNO_3 (pH 4.0) solution. The results from the latter desorbing agent would be relevant in the presence of acid rain or near the roots of plants (the rhizosphere). To compare the desorption behavior of both soils, the amount of Zn desorbed was normalized to the total soil Zn concentrations and plotted as a function of chamber volumes (Fig. 1). The 0.1 mol/L $CaCl_2$ solution caused a substantial amount of Zn to desorb in the initial chamber volumes from both soils. After the initial fast desorption in the first 10 chamber volumes, Zn desorption tailed off to a maximum of 8% of total Zn, which corresponds to 1000 to 2000 ppm Zn.

With the pH 4 solution, 4 to 5 times more Zn was desorbed from both the treated and non-treated soil, up to 35% of total Zn after 80 to 100 chamber volumes (CV). In the first 10 CV, Zn appeared more recalcitrant in the treated soil. Over the reaction range however, Zn desorption from the treated soil exceeded the Zn fraction removed from the untreated fraction (~3%), which may not be statistically significant. After 100 CV, no equilibrium had been reached.

3.3. Zinc Fraction Determined by the BIOMET Biosensor

The bioavailable Zn fraction in the treated Maatheide soil, determined with the bacterial biosensor strain *R. metallidurans* AE1433, was equal to that of the untreated Maatheide soil (~8%, 1010 ± 38 mg Zn kg^{-1} soil dry weight for the treated soil and 1555 ± 10 mg Zn kg^{-1} for the non-treated soil). The bioavailability of a particular metal is often found to be correlated to the exchangeable metal fraction (Vangronsveld et al., 2000; Tibazarwa et al., 2001; Geebelen et al., 2003). This was also the case for the treated and untreated soil samples used in this study. From the desorption studies it followed that the $CaCl_2$ exchangeable fraction was ~7.7% of the total metal fraction, which corresponds to 1050 ppm Zn in the treated soil and 1640 ppm Zn in the non-treated soil. Thus, under the current conditions, 7.7% of the total Zn fraction in the soil is bioavailable in both the treated and non treated soils.

3.4. EXAFS Analysis of Reference Spectra

The raw k^3-weighted EXAFS spectra for the reference Zn minerals and Zn sorption samples are presented in Figure 2. The structural parameters derived from best fitting the spectra are collected in Table 2. The mineral standards chosen, franklinite, willemite, hemimorphite, gahnite and sphalerite, are potential refractory products of the smelting process (Sobanska et al., 1999). Sphalerite (ZnS) is the main ore mineral going into the smelting process. Under basic pH conditions, hydrozincite and smithsonite could possibly form in the soil. Bond distances and coordination numbers derived from non-linear least-square fitting compared well with values reported in the literature for these minerals (Ziegler et al., 2001; Roberts et al., 2002; Waychunas et al., 2002).

Reference spectra of the different Zn containing precipitates that could potentially form in the Zn contaminated soils are collected in Figure 2b. Ford et al. (1999) suggested a transformation sequence of an original transition metal hydroxide precipitate, to a mixed transition metal-Al layered double hydroxide (Me-Al LDH), to a neoformed transition metal phyllosilicate, upon aging. All three possible intermediates were included in the reference database. A Zn-Al LDH was synthesized in the lab and contained ~4 Zn and two Al atoms in the

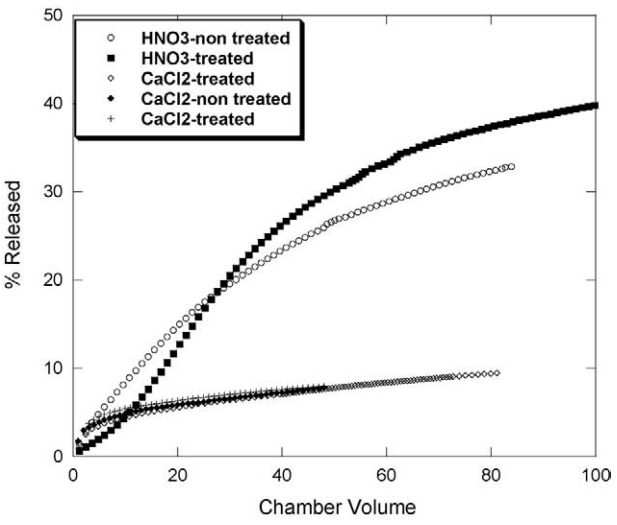

Fig. 1. Percentage of Zn desorbed from the non-treated and treated zinc smelter soils using a 0.1 mol/L $CaCl_2$ solution adjusted to the soil pH (pH 6.5) and a pH 4 HNO_3 solution. CV = chamber volumes. The desorption experiment with the $CaCl_2$ solution of the treated soil sample was repeated in duplicate.

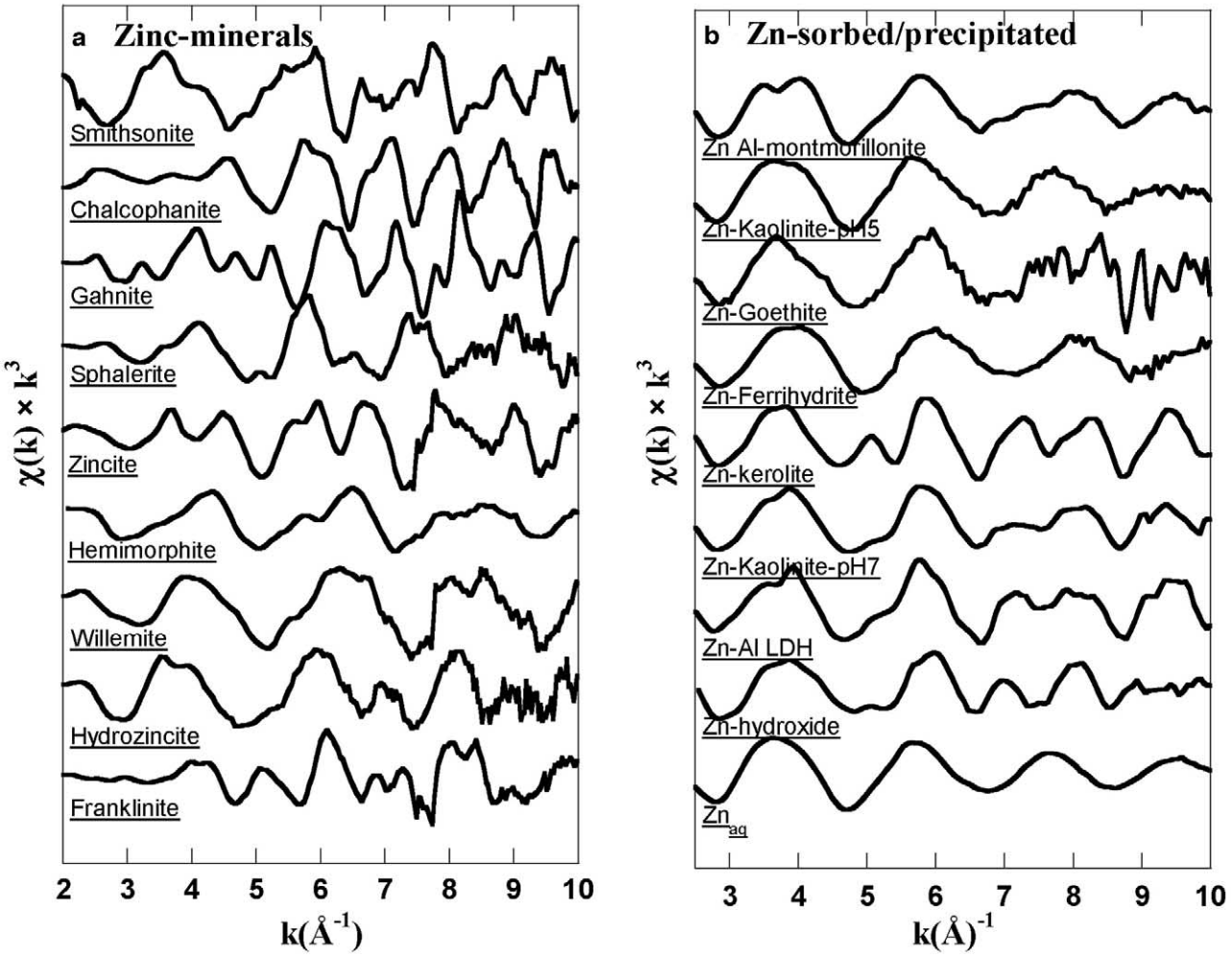

Fig. 2. Zn-K edge k^3 weighted χ-spectra of (a) Zn reference minerals and (b) Zn sorption samples and co-precipitates.

octahedral layers (Table 2). A Zn-phyllosilicate (Zn-kerolite) was best fit with $CN_{Zn\text{-}Zn}$ of 6 in the octahedral layer, and four Si atoms in the tetrahedral layer (Schlegel et al., 2001). A precipitate formed in the presence of kaolinite at pH 7 was found to have four Zn and two Al atoms in the octahedral layer (Nachtegaal and Sparks, 2004).

The raw $k^3\chi(k)$-spectra for the Zn sorption samples are also collected in Figure 2b. The $k^3\chi(k)$-spectrum for aqueous Zn has a sinusoidal shape, whose amplitude decreases with increasing k. Fit results showed that this sinusoidal shape was caused by a single O coordination shell, with $CN_{Zn\text{-}O}$ of 6 and a Zn-O bond distance of 2.07 Å. Zinc formed an edge sharing complex with ferrihydrite, with Zn-Fe distances of 3.41 Å. Zn has ~4 O atoms in the first coordination shell at ~1.99 Å, which is indicative of tetrahedrally coordinated Zn (Waychunas et al., 2002). Upon sorption to goethite, Zn retained its octahedral coordination and formed an inner-sphere sorption complex, with Zn-Fe CN's around one and Zn-Fe bond distances at a significantly shorter distance (3.18 Å) (Nachtegaal and Sparks, 2004). At the kaolinite (a 1:1 clay mineral) surface, Zn binds with the aluminol edge groups of kaolinite at pH 5 with Zn-Al bond distances of ~3.09 Å (Nachtegaal and Sparks, 2004). When sorbed to aluminum modified montmorillonite (a 2:1 clay mineral), a notably shorter Zn-Al bond distance (2.98 Å) was found as compared to sorption onto the aluminol edge sites of kaolinite. The higher $CN_{Zn\text{-}Al}$ (close to 6) suggests that upon sorption to the Al-modified montmorillonite, Zn is incorporated into the Al interlayer of this mineral (Furrer et al., 2001). In addition, Zn-orthophosphate, Zn-humic acid, and Zn-birnessite were tried, but were not detected in the soil.

3.5. Electron Microprobe Analysis

Backscattered electron images (BSE) and selected elemental distributions collected by electron-microprobe analysis are shown in Figures 3a and 3b for the non-treated soil and Figures 3c and 3d for the treated soil. Energy dispersive spectrometry (EDS) survey scanning of grains in the thin sections of both soils indicated that ~80% of the particles present were quartz. Zinc concentrations in the soil thin sections were on the percent level. In both the treated and the non-treated soil thin sections, Zn was mainly found in mixed ZnFe sulfides ([Zn,Fe]S) (Fig. 3a) and iron oxides ($ZnFe_2O_4$) (Fig. 3b), with minor traces of Cu, Ni and Pb also present.

Table 2. Best-fit EXAFS parameters for reference mineral and sorption samples derived from EXAFS analyses.

	First shell				Second shell				
	Atom	CN	R (Å)	σ^2 (Å)^2	Atom	CN	R (Å)	σ^2 (Å)^2	ΔE_0 (eV)
Minerals									
Franklinite	O	4.1	1.98	0.003	Zn/Fe	11	3.50	0.004	3.00
Willemite	O	3.8	1.94	0.003	Si	1.5	3.18	0.007	1.91
					Zn	2.1	3.25	0.007	
Hemimorphite	O	3.6	1.93	0.005	Zn	3.0	3.01	0.008	–2.35
					Si	2.3	3.33	0.008	
Zincite	O	3.9	1.96	0.003	Zn	14.3	3.22	0.010	–2.39
Sphalerite	S	4.3	2.34	0.007	Zn	12.0	3.83	0.015	3.11
Hydrozincite	O	3.4	1.98	0.005	Zn	3.0	3.12	0.010	–4.25
Smithsonite	O	6.0	2.10	0.010	C	3.8	2.99	0.007	2.97
					Zn	3.8	3.65	0.007	
Gahnite	O	3.6	1.97	0.004	Al	12.5	3.38	0.008	–5.31
					Zn	5.1	3.54	0.008	
Co-precipitates									
Zn-Al-LDH	O	6.2	2.06	0.008	Zn	4.3	3.09	0.010	0.06
					Al	2.2	3.10	0.010	
Kerolite	O	6.2	2.06	0.006	Zn	6.2	3.10	0.006	0.10
					Si	4.4	3.23	0.006	
Zn-kaolinite pH7	O	5.2	2.03	0.010	Zn	4.9	3.10	0.010	0.64
					Al	2.6	3.12	0.010	
Zn-hydroxide	O	1.9	2.02	0.013	Zn	2.3	3.15	0.016	1.15
Sorption samples									
Zn_{aq}	O	6.0	2.07	0.009					
Zn-ferrihydrite	O	4.6	1.99	0.008	Fe	1.6	3.41	0.011	–0.16
Zn-goethite	O	6.0	2.04	0.006	Fe	1.0	3.18	0.014	0.62
Zn-kaolinite pH5	O	6.4	2.06	0.011	Al	1.3	3.09	0.010	0.46
Zn-Al-mont. pH6	O	5.2	2.05	0.010	Al	5.8	2.98	0.005	0.75

CN = coordination number (±20%; Scheidegger et al., 1997); R = inter-atomic distance (±0.02 Å for first shell and ±0.05 Å for the second and third shell; Scheidegger et al., 1997); σ^2 (Å^2) = Debye Waller factor; ΔE_0 = phase shift.

Occasionally, Zn was also found associated with Si and Al (Figs. 3c and 3d). The Zn-Si associations (Fig. 3c) have a mainly unaltered hexagonal shape, suggesting that this mineral is either newly formed in the smelter (hemimorphite $[Zn_4Si_2O_7(OH)_2 \cdot H_2O]$ or willemite $[Zn_2SiO_4]$) or pseudomorphic. Strong associations of Zn with Al (Fig. 3d) were also found, probably as a result of Zn included into refractory minerals such as gahnite ($ZnAl_2O_4$), in pseudomorphic Zn-Al associations formed after gahnite or in mixed Zn-Al precipitates neoformed in the soil.

The detection limit of the microprobe for Zn under the conditions used in this study is ~0.5 wt.%, therefore the electron microprobe could only probe the Zn hotspots, i.e. the main Zn mineral associations. Lower Zn concentrations, i.e. Zn re-adsorbed to mineral phases will not be detected, although this Zn fraction can play a very important role in the overall Zn speciation (Roberts et al., 2002). With micro-focused synchrotron-based X-ray fluorescence (μ-SXRF) significantly lower Zn concentrations can be probed. However, the disadvantage of μ-SXRF at beamline 10.3.2 at the ALS, where we collected our spectra, is that information on associations of Zn with elements of low atomic weight, such as Si or Al, can not be obtained due to the limitations of the fluorescence detector.

3.6. Synchrotron Micro-XRF and Micro-EXAFS of Soil Thin Sections

Several regions in the thin sections were examined in detail by μ-SXRF. Four μ-SXRF maps of the treated and four of the non-treated soil thin sections, representing the complete chemistry of Zn in both soils are shown in Figure 4a for the treated and Figure 5a for the non treated soils. The maps are shown as RGB tricolor maps. In these images R (red) represents the distribution of iron, G (green) the distribution of Cu and B (blue) the distribution of Zn. The color values of each pixel are proportional to the fluorescence yield and therefore relative concentrations of the three elements. Gray or white areas contain comparable amounts of Fe, Zn and Cu. The overall brightness of a region is related to the sum of the concentrations and the hue is related to the difference (Manceau et al., 2002).

Zinc, Cu, Fe, Mn, Ni, Ti, Co, Ca and K were simultaneously mapped. Due to limitations of the fluorescence detector, light elements could not be mapped in μSXRF. The μ-SXRF maps of the thin sections show the heterogeneous distribution of Zn in both the treated and non-treated soil samples. For example, Zn was found at edges of Fe rich particles (e.g. Fig. 5a, region 2), correlated with Fe and Cu (Fig. 4a region 4), mostly in diffuse spots (e.g. Fig. 5a, region 3) or concentrated regions just by itself (e.g. Fig. 5a, region 4). Specific information on the chemistry and local bonding environment of Zn in different locations in the SXRF maps was obtained from μ-focused EXAFS spectroscopy on selected spots.

Principal component analysis (PCA) was performed on the complete set of μ-EXAFS spectra collected from the treated soil (17 in total, including the bulk soil spectrum) and the spectra set of the non-treated soil (13 spectra in total, including the bulk soil spectrum) to determine the number of independent

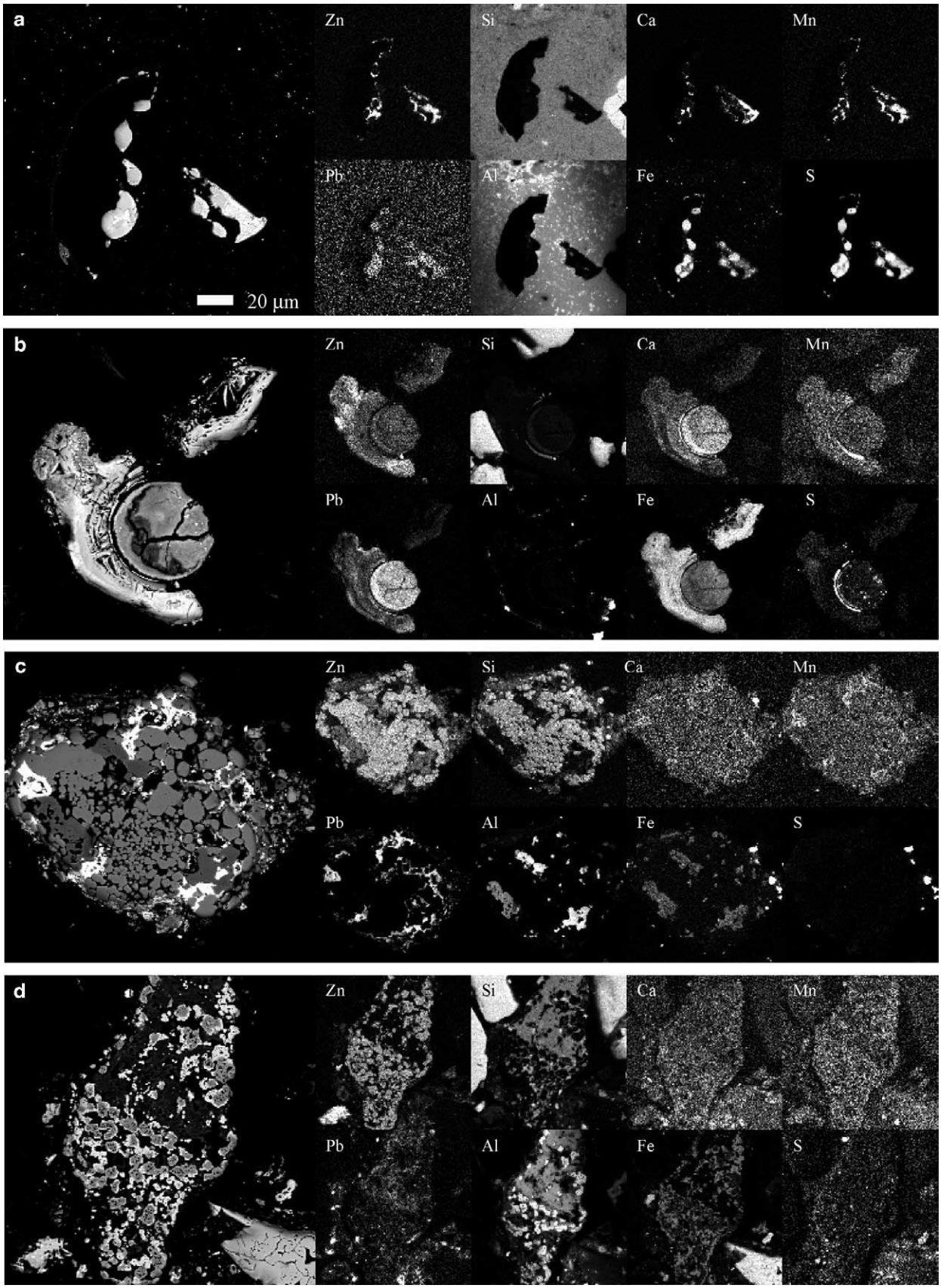

Fig. 3. Backscatter electron images (large) and elemental distribution maps (small images) of selected particles in the non-treated (a, b) and treated (c, d) zinc smelter soil.

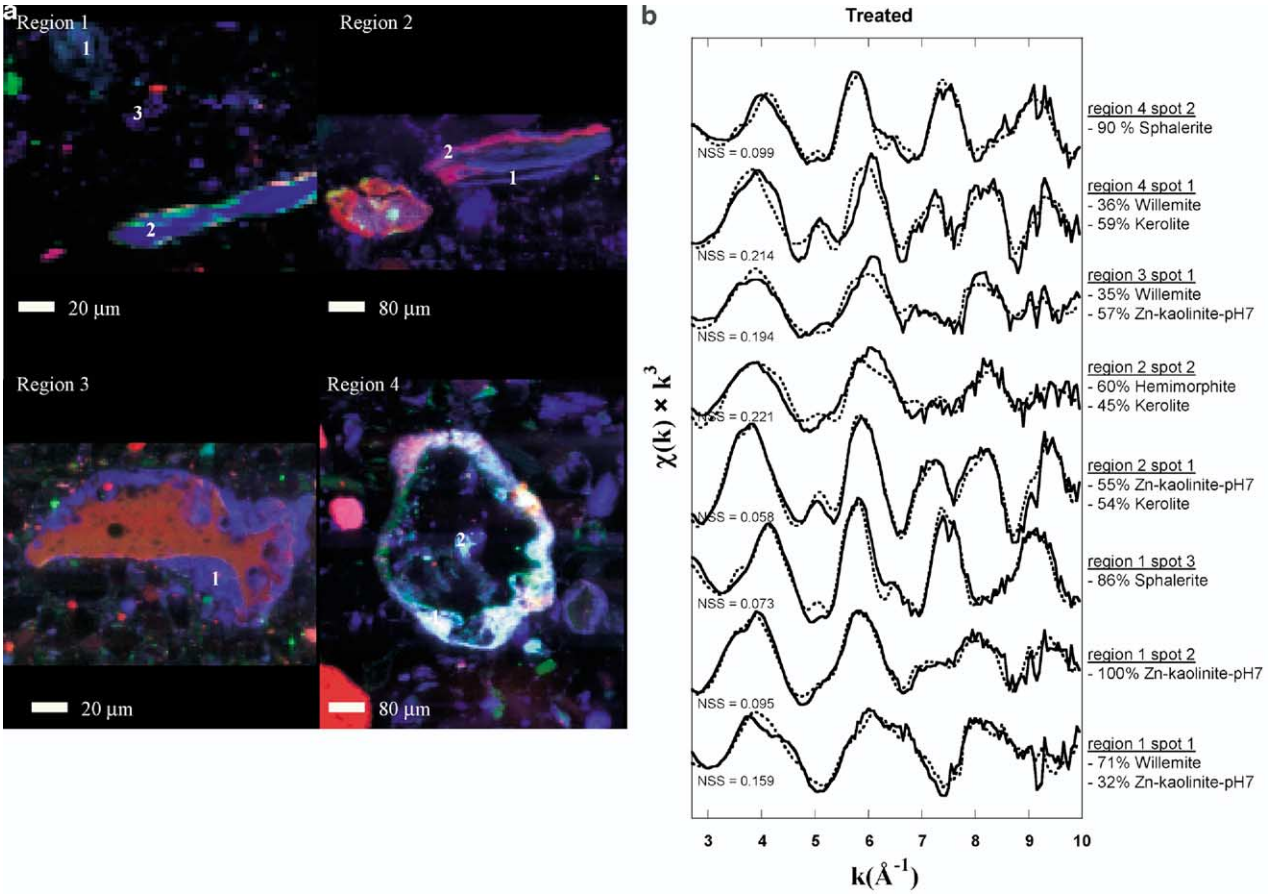

Fig. 4. (a) μ-SXRF tricolor maps for the treated soil samples. The numbers indicate the spots where μ-EXAFS spectra were collected. Red is indicative of the distribution of iron, green of copper and blue of zinc. (b) μ-EXAFS spectra from selected spots on thin sections from the treated soil. The solid line indicates the raw $k^3\chi(k)$ data and the dotted line indicates the best fits obtained with a linear fitting approach.

components contained in the set of spectra. This approach is useful for the analysis of natural samples containing multiple forms of Zn, because the number and nature of these forms cannot be assumed a priori (Isaure et al., 2002). Principal component analysis indicated that three to four principal components were needed to reproduce the data set of the treated soil and four components were necessary to reproduce the data set of the non-treated soil. All μ-EXAFS spectra could be reproduced very well with these 4 principal components (normalized sum square (NSS) between 0.080 and 0.165 for the treated soil and 0.037 and 0.126 for the non-treated soil, data not shown).

The four most likely Zn species in both the treated and non-treated spectral data sets were then identified by target transformation of reference spectra from the database presented in section 3.4. The SPOIL factors, which indicate how well a Zn reference spectrum matched to the principal components, for the different references in our database soils are collected in Table 3. The best target transformations for the treated soil were obtained with hemimorphite, willemite, kerolite/LDH/Zn kaolinite pH7, and sphalerite. Kerolite, used as a proxy for Zn incorporated in a neoformed phyllosilicate precipitate, Zn-kaolinite-pH 7 and LDH, used as a proxy for Zn incorporated in a neoformed layered double hydroxide precipitate formed near the kaolinite surface or homogeneously in solution respectively, all share a similar structure, they will give similar good fits. Therefore, we opted to only use one of the three, spectrally very similar, reference spectra (Fig. 2b) for our fits, in this case kerolite and add one of the other three when it gives a significantly better fit. Good spectral fits for the non-treated soil were obtained with hemimorphite, gahnite, sphalerite and again LDH/kerolite/Zn-kaolinite-pH7.

As an extra check we merged the datasets of the treated and non-treated soils and found that we needed five principal components to reproduce the big dataset. The target transformation showed willemite, hemimorphite, gahnite, sphalerite and LDH/phyllosilicate as best fits, basically confirming the individual fits for the treated and non-treated samples.

The proportion of each Zn reference species, as identified by target transformation of the principal components, in the various μ-EXAFS spectra was determined by linear combination fitting (LCF). Only the Zn references which were not eliminated by the target transformation were included into the fit. The solid lines in μ-EXAFS Figures 4b and 5b represent the raw $k^3\chi$ spectra of the treated and non-treated soils respectively and the dotted lines are the best fits to the raw data. The normalized sum square (NSS) values listed with each spectrum, indicates the goodness of the LCF fits.

Four selected SXRF maps from the thin sections of the

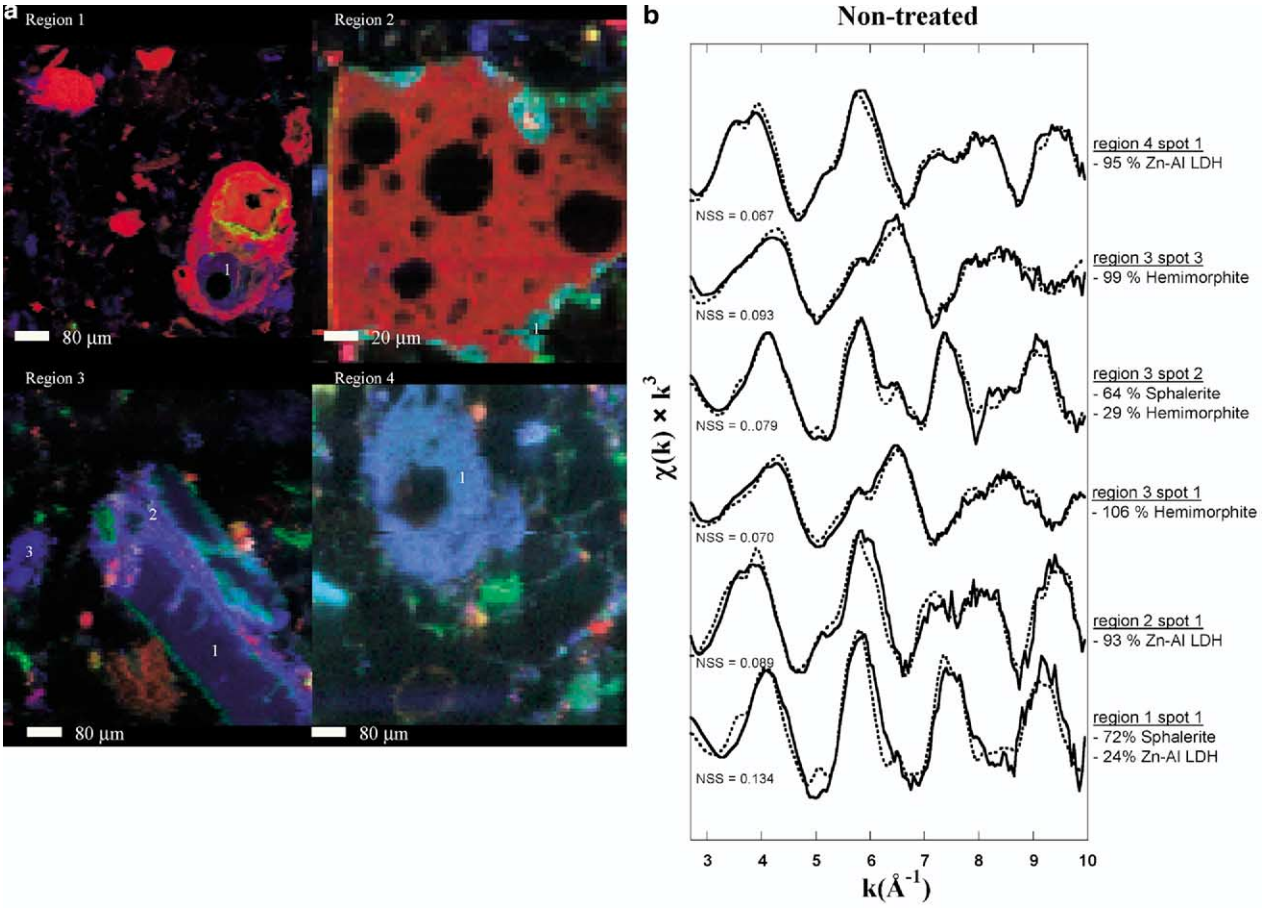

Fig. 5. (a) μ-SXRF tricolor maps for the non-treated soil samples. The numbers indicate the spots where μ-EXAFS spectra were collected. Red is indicative of the distribution of iron, green of copper and blue of zinc. (b) μ-EXAFS spectra from selected spots on thin sections from the non-treated soil. The solid line indicates the raw $k^3\chi(k)$ data and the dotted line indicates the best fits obtained with a linear fitting approach.

treated soil, covering the complete range of chemical species found in the treated soil, are shown in Figure 4a and μ-EXAFS spectra of selected spots in the SXRF maps are shown in Figure 4b. A Zn and Cu rich region in region 1 (region 1 spot 1, Fig. 4a) was best fitted with a combination of willemite and the Zn precipitate formed in the presence of kaolinite (Zn-kaolinite-pH7) (Fig. 4b). Cu in this region could result from the inclusion of Cu in the neoformed precipitate. The bright elongated Zn particle, with Cu at the rims (region 1 spot 2) was best fitted by Zn-kaolinite-pH7. The μ-EXAFS spectrum of a small bright Zn particle (region 1 spot 3) coincided with the spectrum of sphalerite (ZnS). In the second XRF region (region 2), again a long elongated Zn rich particle was found, with a higher concentration of Fe at the upper edge. The area in this particle with mostly Zn was best fitted with a mixture of kerolite and Zn-kaolinite-pH7 (region 2 spot 1), although the kerolite by itself already gave a very good fit. This indicates that a precipitate was formed which is not 100% similar to kerolite and not 100% similar to a precipitate formed in the presence of kaolinite, but rather carries the characteristics of both. The Fe rich region on the elongated particle was fitted with kerolite (region 2 spot 2). That phase however did not quite fit the spectrum well by itself. By including a second phase, hemimorphite, the fit strongly improved. The NSS of this two component fit is still quite high, indicating that we did not manage to positively identify the second species going into the fit using the constraints of the four components selected. The second component is most likely correlated to a Fe rich mineral (as indicated by the XRF maps) and Zn in this component is tetrahedrally coordinated (as in hemimorphite). When we attempted to fit the spectrum, without constraints on the references going into the fit, we found that Zn-sorbed ferrihydrite (also tetrahedrally coordinated) best fitted the spectrum. However, the NSS was still ~0.2 which was not a big improvement of the fit presented here. Region 3 (Fig. 4a) is characterized by a large iron rich particle (red color) surrounded by a concentrated Zn region. This Zn rich region (region 3 spot 1) was best fitted with Zn-kaolinite-pH7 and again a tetrahedral Zn compound, in this case willemite. In the last selected SXRF map for the treated soil, region 4, we found a Fe, Cu and Zn rich band. Region 4 spot 1 was fitted with a mixture of kerolite and willemite. The small Zn and Cu rich spot in the middle of the picture (region 4 spot 2) was clearly sphalerite. That the fits with sphalerite in region 4 spot 1 and region 1 spot 3 only added up to 90% could be due to over-absorption in this highly-concentrated Zn particle.

Table 3. SPOIL factors for the reference spectra constructed from principal components.

Reference	Treated	Non-Treated
Franklinite	4.6	5.1
Willemite	**1.8**	4.1
Hemimorphite	**1.6**	**1.5**
Zincite	7.7	8.9
Sphalerite	**2.5**	**1.8**
Hydrozincite	3.9	4.8
Smithsonite	9.9	5.1
Gahnite	9.4	**1.6**
LDH	**2.2**	**2.2**
Kerolite	**1.1**	2.9
ZnOH	4.5	6.4
Zn-nitrate	5.2	3.4
Zn-birnessite	4.2	4.5
Zn-ferrihydrite	3.9	3.1
Zn-goethite	6.6	6.0
Zn-fulvic acid	5.5	4.4
Zn-kaolinite pH5	6.3	4.8
Zn-Al mont	3.6	3.0

SPOIL factors < 1.5 indicate an excellent fit, 1.5 to 3 a good fit, values of 3 to 4.5 a fair and of 4.5 to 6 a poor fit and factors > 6.0 are unacceptable. In bold are the references used in the fits.

Figure 5a shows four selected SXRF maps from the two thin sections of the non-treated soil, covering the complete range of chemical species found in the non-treated soil thin sections. Figure 5b contains the LCF fitted μ-EXAFS spectra of selected spots in the SXRF. Region 1 (Fig. 5a) contains a Fe rich particle containing a Zn-rich area. This area was best fitted with sphalerite and LDH. A second region (region 2) contained a large iron-rich particle, with a high concentration of Zn and Cu at the rims. A micro-EXAFS spectrum taken at this Zn/Cu-rich region suggested that an LDH had formed at the rims of this iron rich particle. In a third SXRF region we found one extremely bright Zn particle (region 3 spot 3), a long elongated less concentrated Zn region, where also locally some Fe and Cu are concentrated (region 3 spot 2) and a more-concentrated Zn rich region on this particle (region 3 spot 1). Both region 3 spot 1 and region 3 spot 3 turned out to be hemimorphite. Region 3 spot 2 was a mixture between hemimorphite and sphalerite. The sphalerite (ZnS) could also incorporate Fe and Cu, thus the concentration of Fe and Cu in region 3 spot 2 on the SXRF maps is of no surprise. In region 4 a large Zn rich particle was found (region 4 spot 1). This particle was perfectly fit by a Zn-LDH.

3.7. Bulk EXAFS Analysis

Bulk EXAFS spectra of both the treated and non-treated soils were collected to quantify the major Zn form in the non-treated soil and in the treated soil (Fig. 6). The raw $\chi(k)k^3$ spectra were linearly fit by combinations of reference spectra, which were positively identified in the PCA analysis of the μ-EXAFS and the bulk EXAFS spectra combined. With this approach, one could estimate the major phases which contribute to the overall spectrum. In Figure 6a the bulk spectra of the treated and non-treated soil samples are compared. Both spectra look very similar. The phase of the first oscillation and to a lesser extent of the second oscillation of the treated-soil spectrum is shifted to lower wavelengths compared to the spectrum of the non-treated soil. This suggests a higher concentration of tetrahedral Zn in the treated soil, compared to the non-treated soil. Also, a small oscillation between 7 and 8 Å is more pronounced in the treated sample compared to the non-treated sample. It should be noted that LCF becomes progressively harder when bulk soils are fitted, since more species overlap to give the final spectrum. This is illustrated below in the fits for the treated and non-treated soil samples.

The non-treated bulk sample was reasonably well fitted with just two components, octahedral Zn in LDH and tetrahedral zinc in hemimorphite (Fig. 6b). However, the fit is a little bit out of phase with the non-treated soil spectrum and especially the second oscillation is fitted poorly. The fit significantly improved (>50% in the NSS) when a third component, gahnite, was included into the fit (Fig. 6c). All features in the spectra are well reproduced, except for the amplitude of the first and second oscillations. Gahnite was already positively identified in the PCA analysis of the non-treated samples. It turns out to be a major component in the bulk soil, whereas it was not found in the micro-EXAFS spectra. This shows that even though we had 12 micro-EXAFS spectra from the non treated soil we could still miss a major component in the micro-EXAFS analysis.

The treated soil was well fitted with just two components: the precipitate formed in the presence of kaolinite and willemite (Fig. 6d). The fit of the treated soil spectrum improved by 20% when a third component, kerolite, was included in the fit (Figs. 6e and 6f). In particular, the little oscillation between 7 and 8 $Å^{-1}$ was much better reproduced. It turned out that willemite and hemimorphite were almost interchangeable in the fit, without altering much of the final fit. This illustrates that LCF is not that species sensitive when applied to a bulk soil sample. Attempts to include a fourth component, such as sphalerite (which was found in two spots in the micro-EXAFS spectra (Fig. 4b)) did not improve the final fit. This shows that micro-EXAFS is able to pick up minor Zn species, which might not be important in the total Zn fraction.

4. DISCUSSION

4.1. Zinc Speciation

Several slag-related Zn mineral phases, i.e. willemite, sphalerite, gahnite and hemimorphite, were identified in the treated and non-treated soils by bulk and micro-focused EXAFS spectroscopy. These minerals have been deposited on the soil mainly by fall out from the chimney stack of the smelter. Sphalerite (ZnS) minerals are remnants of the raw ore that by-passed the pyrometallurgical smelting process due to incomplete oxidation of ZnS (up to 20%), generating ZnS containing slags (Isaure et al., 2002). Willemite (Zn_2SiO_4) is a high-temperature anhydrous silicate that originates from the smelting process. Likewise, hemimorphite ($Zn_4Si_2O_7[OH]_2 \cdot H_2O$) and gahnite ($ZnAl_2O_4$) could have been formed in the smelting process. Linear combination fitting of the EXAFS spectra of the treated and non-treated bulk soils indicated that of the four smelter minerals, sphalerite plays a minor role in the overall Zn speciation and gahnite was only present in minor quantities in the non-treated soils. Sphalerite was identified in

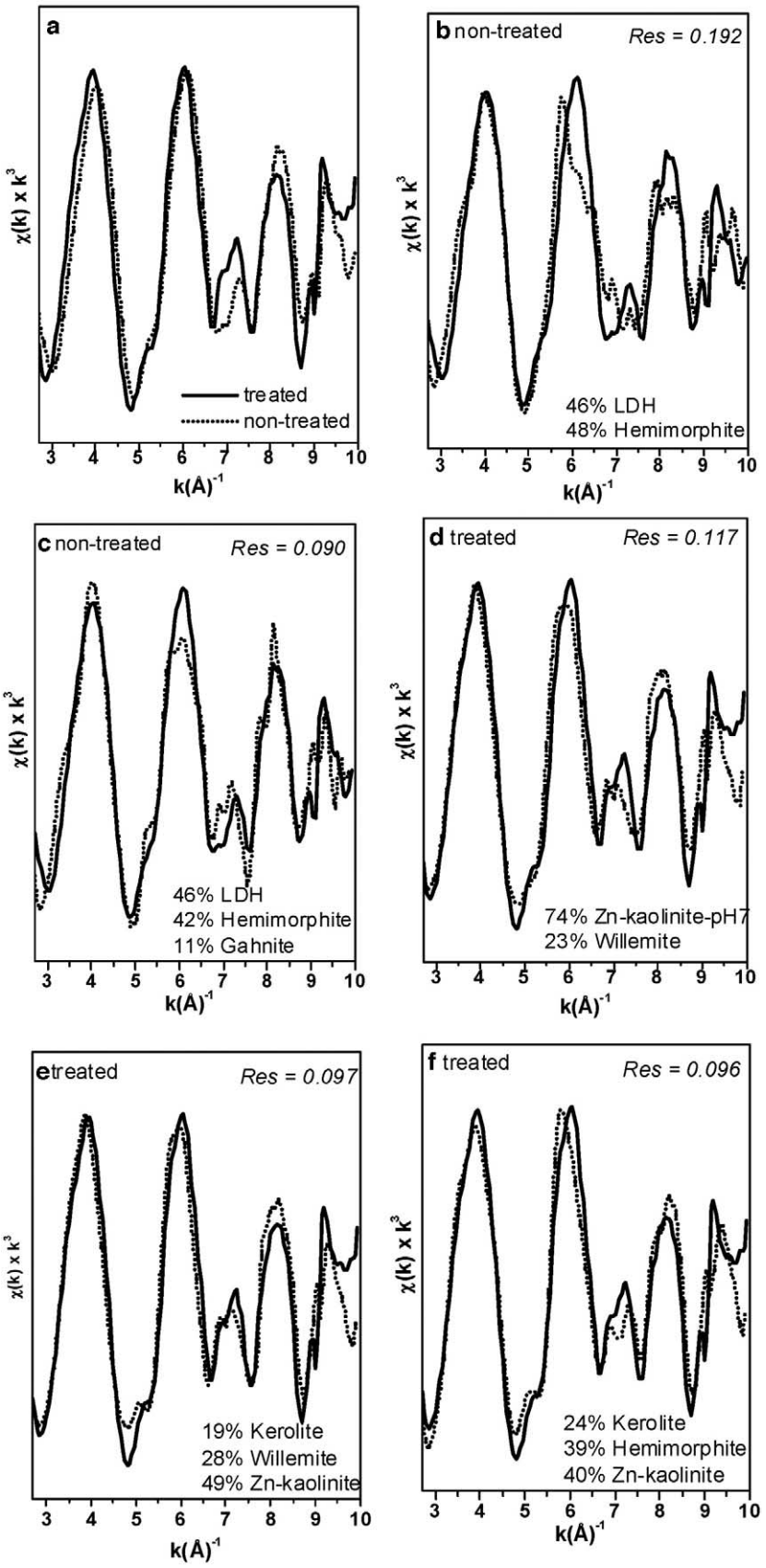

Fig. 6. EXAFS spectra of the treated and the non-treated bulk soil. The solid lines indicate the raw $k^3\chi(k)$ data and the dotted line indicates the best fits obtained with a linear fitting approach.

the micro-EXAFS spectra, since this mineral shows up as intense Zn hot spots in the SXRF maps.

The lead isotopes confirmed that most of these 'primary' smelter 'fall-out' minerals were deposited between 30 and 45 yr ago. Whereas our bulk soil EXAFS analysis indicated that these primary minerals make up only 30% to 50% of the current Zn fraction in the soil, a significant percentage of the Zn (50%–70% according to LCF of the bulk soils EXAFS spectra) is distributed into secondary Zn phases. These results suggest that the primary slag related minerals, some already deposited on the soil more than a century ago, have been significantly weathered over time. Sphalerite (ZnS) in particular may have oxidized and dissolved in the oxygenated soil environment, suggesting that these processes (oxidative-dissolution) of redox sensitive materials are important reactions controlling the solubility of Zn.

Linear combination fitting of the bulk soils and detailed analyses of the soil thin sections with μ-focused EXAFS spectroscopy indicated that upon weathering of the primary polluting minerals Zn is mainly incorporated into neoformed Zn precipitates. These precipitates were very similar in structure to our reference phases produced in the lab; Zn-Al layered double hydroxide and Zn-kerolite (a Zn containing phyllosilicate). In the non-treated soil the precipitate phase formed was similar to a layered double hydroxide (Zn-Al LDH), whereas the precipitate formed in the treated soil resembled more a Zn-phyllosilicate (kerolite).

The difference in the type of precipitate formed in the treated soil compared to the non-treated soil suggests that in the treated soil, where the local pH varied between 7.3 and 7.9 at the time of the treatment (Vangronsveld et al., 1995), more silica was available for the formation of a Zn-phyllosilicate. The higher pH of the soil solution at the time of remediation may have enhanced this process. It should be noted that the spectral differences between a layered double hydroxide and a phyllosilicate are small. Only with polarized EXAFS spectroscopy can a definite distinction between these two types of precipitates be made (Manceau et al., 2000). The main points to be made here however are that these precipitates do form, are poorly-crystalline in nature and thus will not be picked up with conventional XRD, and constitute ~60% of the total Zn fraction in both the treated and non-treated smelter soil.

This difference in pH at the time of remediation might also have led to an increased weathering of the gahnite ($ZnAl_2O_4$) in the treated soil. This might explain why gahnite was only found in the non-treated soil and not in the treated soil.

Our observations on the Zn speciation in the non-treated soil correlate well with a study by Manceau et al. (2000) on Zn-contaminated smelter soils from the same geographical area. They used conventional XRD, bulk EXAFS and P-EXAFS spectroscopy to speciate Zn in the bulk soils (pH ~ 6.5), and found willemite and hemimorphite as the primary polluting Zn minerals in this soil. Upon weathering, Zn was found predominately incorporated into neoformed Zn-containing phyllosilicates and to a lesser extent bound to Mn and Fe (hydr)oxides. At a significantly lower pH (~5), Roberts et al. (2002) studied the Zn speciation in different horizons of a smelter contaminated soil. These authors found Zn mostly bound to Al-groups of the clay minerals and to a lesser extent to Fe and Mn (hydr)oxides. Under these conditions, no indication of the presence of Zn containing precipitates was found, suggesting that the formation of these precipitates only takes place at near-neutral pH. Contrary to these studies we did not only speciate Zn in the contaminated area but also tried to validate to what extent the remediation attempt changed the speciation in the treated soil.

4.2. Long Term Zinc Bioavailability and Mobility

The higher intrinsic Zn concentration in the non-treated soil samples lead to a higher Zn concentration in the exchangeable fraction and therefore a higher Zn bioavailability and toxicity in the non-treated soil, as was confirmed using the *R. metallidurans* AE1433 biosensor. The amount of bioavailable Zn in both soils was ~8% of total Zn, which agreed well with the exchangeable metal fraction observed in the stirred flow desorption experiments.

It is important to monitor Zn release under changing environmental conditions, e.g. acidification of the soil, before making any predictions on long term Zn mobility. The striking similarities in Zn speciation suggests that both the treated and non-treated soil should behave similarly under acidification. Using the pH 4.0, HNO_3 solution, 30% to 40% of total Zn was desorbed from the treated and non-treated soils. Even after 100 chamber volumes the reaction was not complete, indicating an additional fraction could be desorbed under acidic conditions. Therefore we suggest that the newly formed Zn-containing precipitates, which constitute 50% to 70% of the total Zn fraction, are not stable under acidic conditions. As long as the pH buffering capacity of the soil is high, Zn released from weathering of primary minerals may be sequestered by neoformed precipitates such as LDH's or phyllosilicates. But when the pH is lowered, for example due to (acid) rain fall, or due to a localized lower pH in the rhizosphere of plants exuding acidifying compounds, this Zn fraction could become bioavailable. The initial faster release of Zn by the non-treated soil compared to the treated soil might be explained by the presence of a more stable Zn-phyllosilicate phase in the treated soil compared to a Zn-Al LDH neoformed precipitate in the non-treated soil.

The fact that the vegetation was restored at the remediated site (Vangronsveld et al., 1995) appears striking based on our results, which show that presently there is no significant difference in speciation between both soils and that the bioavailable Zn fraction in both the treated and the non-treated soil samples exceeded 1000 ppm Zn. Two factors might have contributed to the restoration of the ecosystem at the remediated site. Firstly, the additives applied at the time of remediation lead to a temporary decrease in the exchangeable Zn fraction, by the formation of Zn precipitates. Biosensor tests carried out on soils to which cyclonic ash was added showed a significant decrease in metal availability and phytotoxicity for at least 3 yr (Vangronsveld et al., 2000). Secondly the addition of organic matter may have helped with restoring the ecosystem at the treated site. The soils were extremely poor in organic matter, which made it very difficult for any species to colonize and survive. The addition of compost favored the development of a plant cover in several ways: (1) a decrease in bioavailability of metals (due to complexing of free metal forms in dissolved organic matrices), and (2) an increase in water retention

capacity and nutrient availability. Once a plant cover was established, this resulted in a continuous flow of additional organic matter into the soil, which in turn could have contributed to further nutrient availability and increased water retention. A normalization of the below-ground food-web, as expressed by the numbers and diversity of organisms and of metabolic functioning, was observed on the treated site (Bouwman et al., 2001; Bouwman and Vangronsveld, 2004). The increasing occurrence of non-metal-tolerant plants on the treated area (Vangronsveld et al., 1996, confirmed by field observations in 2001 and 2003) may also be partly related to the well-developed mycorrhizal community (Vangronsveld et al., 1996). Increased metal tolerance of mycorrhiza and their beneficial effects on host-plants without increased metal tolerance growing on metal contaminated substrates was shown by Adriaensen et al. (2004).

We found a strong incorporation of Zn into newly formed phases in both the treated and non treated soil samples, which probably led to a decrease in the bioavailability of metals in the treated and non-treated soils. An indirect argument for the natural attenuation of bioavailable metals in the non-treated soil is the increasing colonization of the non-treated area by metal-tolerant plants that has been observed since 1998.

5. CONCLUSIONS

The goal of this study was to speciate Zn both in a contaminated soil and its remediated counterpart, in order to elucidate the long-term effects of remediation on Zn speciation and Zn bioavailability. We were especially interested in the role that neoformed Zn precipitates can play in the reduction of the bioavailable Zn fraction. Comprehensive bulk and micro-focused EXAFS studies showed no significant differences in Zn-speciation between the contaminated smelter soil and the remediated area treated 12 yr ago with cyclonic ash and compost. Pb isotope signatures indicated that most of the Zn present in the soil was deposited 30 to 45 yr ago downwind from the Zn smelter. Only 30% to 50% of total Zn is still present in primary, smelter-related, phases such as willemite, hemimorphite and gahnite. These smelter related minerals have weathered over time. Especially the oxidation of sphalerite and the weathering of gahnite in the higher pH remediated area might have contributed to a high Zn availability in the treated soil. Neoformed Zn containing phases, whether a Zn-Al LDH (non-treated soil) or a Zn-phyllosilicate (treated soil), made up the remaining 50% to 70% of total Zn in the treated and non-treated soils. Only with state-of-the-art techniques such as EXAFS spectroscopy could these poorly-crystalline mineral phases be distinguished in these soil samples. Neoformed precipitates are therefore very important at near neutral pH in highly contaminated soils and should be considered when modeling Zn speciation.

The incorporation of Zn into stable neoformed precipitates at higher pHs lead to a significant natural attenuation of the exchangeable/bioavailable Zn fraction at the pH of the soil, as was confirmed using the *R. metallidurans* AE1433 biosensor. The formation of neoformed precipitates however, may not lead to a permanent sequestration of Zn from the soil solution. When the pH of the soil was lowered, most Zn was released from the soil. Since Zn containing precipitates constitute 50% to 70% of the total Zn fraction, these results suggest that the precipitates were not thermodynamically stable at lower pH. The pH 4 stirred flow desorption results obtained suggest that also on the additive treated soil a long-term stable fixation of Zn is questionable under acidifying conditions.

Acknowledgments—The authors would like to thank Drs. A. Manceau, A. Voegelin and D.R. Roberts for kindly providing some of the EXAFS spectra of Zn references used in this study, and Dr. R. Kretzschmar, Dr. M. Gräfe and David McNear for proofreading the manuscript and three anonymous reviewers for their excellent comments and suggestions. We acknowledge the staff of beamline X11A at the National Synchrotron Light Source (NSLS) in Upton NY for their assistance in the collection of the EXAFS data. We are grateful to the ALS and the NSLS for the provision of beam-time. D. van der Lelie is presently supported by Laboratory Directed Research and Development funds at the Brookhaven National Laboratory under contract with the U.S. Department of Energy. The ALS is supported by the Director, Office of Energy Research, Office of Basic Energy Sciences, Materials Sciences Division of the U.S. Department of Energy, under contract No. DE-AC03-76SF00098.

Associate editor: L. Warren

REFERENCES

Adamo P., Dudka S., Wilson M., and McHardy W. (1996) Chemical and mineralogical forms of Cu and Ni in contaminated soils from the Sudbury mining region and smelting region. *Canada Environ. Pollut.* **91,** 11–19.

Adriaensen K., van der Lelie D., Van Laere A., Vangronsveld J., and Colpaert J. V. (2004) A zinc-adapted fungus protects pines from zinc stress. *N. Phytol.* **161,** 549–555.

Bertsch P. M. and Hunter D. B. (1998) Elucidating fundamental mechanisms in soil and environmental chemistry: The role of advanced analytical spectroscopic, and microscopic methods. *Soil Sci. Soc. Am. Spec. Publ.* **55,** 103–122.

Brümmer G. W., Tiller K. G., Herms U., and Clayton P. M. (1983) Adsorption-desorption and/or precipitation-dissolution processes of Zn in soils. *Geoderma* **31,** 337–354.

Boisson J., Ruttens A., Mench M., and Vangronsveld J. (1999) Evaluation of hydroxyapatite as a metal immobilizing soil additive for the remediation of polluted soils. Part 1. Influence of hydroxyapatite on metal exchangeability in soil, plant growth and plant metal accumulation *Environ. Pollut.* **104,** 225–233.

Bouwman L. and Vangronsveld J. (2004) Rehabilitation of the nematode fauna in a phytostabilized heavily zinc contaminated sandy soil. *J. Soils Sed.* **4,** 17–23.

Bouwman L., Bloem J., Römkens P. F. A. M., Boon G. T., and Vangronsveld J. (2001) Beneficial effect of the growth of metal tolerant grass on biological and chemical parameters in copper- and zinc contaminated sandy soils. *Minerva Biotech* **13,** 19–26.

Calmano W., Mangold S., and Welter E. F. (2001) An XAFS investigation of the artifacts caused by sequential extraction analyses of Pb-contaminated soils. *J. Anal. Chem.* **371,** 823–830.

Chlopecka A. and Adriano D. C. (1997) Inactivation of metals in polluted soils using natural zeolite and apatite. In *Proc. 4th Int. Conf. Biogeochem. Trace Elem.*, Berkeley, CA.

Corbisier P., Thiry E., and Diels L. (1996) Bacterial biosensors for the toxicity assessment of solid waste. *Environ. Toxicol. Wat. Qual.* **11,** 171–177.

Corbisier P., van der Lelie D., Borremans B., Provoost A., de Lorenzo V., Brown N., Lloyd J., Hobman J., Csöregi E., Johansson G. and Mattiasson B. (1999) Whole cell- and protein-based biosensors for the detection of bioavailable heavy metals in environmental samples. *Anal. Chim. Acta* **387,** 235–244.

Eick M. J. and Fendorf S. E. (1998) Reaction sequence of nickel(II) with kaolinite: Mineral dissolution and surface complexation and precipitation. *Soil Sci. Soc. Am. J.* **62,** 1257–1267.

Ford R. G. and Sparks D. L. (2000) The nature of Zn precipitates formed in the presence of pyrophyllite. *Environ. Sci. Technol.* **34,** 2479–2483.

Ford R. G., Scheinost A. C., Scheckel K. G., and Sparks D. L. (1999) The link between clay mineral weathering and the stabilization of Ni surface precipitates. *Environ. Sci. Technol.* **33,** 3140–3144.

Furrer G., Scheidegger A., Plötze M., Kahr G., Studer B., Lothenbach B., and Schulin R. (2001) Specific immobilization of heavy metals in soil using modified montmorillonite. *Mitt. Dtsch. Bodenkundl. Ges.* **96,** 181–182.

Geebelen W., Adriano D. C., van der Lelie D., Mench M., Carleer R., Clijsters H. and Vangronsveld J. (2003) Selected bioavailability assays to test the efficacy of amendment-induced immobilization of lead in soils. *Plant Soil* **249,** 217–228.

Gruebel K. A., Davis J. A., and Leckie J. O. (1988) The feasibility of using sequential extraction techniques for arsenic and selenium in soils and sediments. *Soil Sci. Soc. Am. J.* **52,** 390–397.

Gworek B. (1992a) Inactivation of cadmium in contaminated soil using synthetic zeolites. *Environ. Pollut.* **75,** 269–271.

Gworek B. (1992b) Lead inactivation in soils by zeolites. *Plant Soil* **143,** 71–74.

Henderson P. J., McMartin I., Hall G. E., Percival J. B., and Walker D. A. (1998) The chemical and physical characteristics of heavy metals in humus and till in the vicinity of the base metal smelter at Flin Flon, Manitoba, Canada. *Environ. Geol.* **34,** 39–58.

Isaure M. P., Laboudigue A., Manceau A., Sarret G., Tiffreau C., Trocellier P., Lamble G., Hazemann J. L., and Chateigner D. (2002) Quantitative Zn speciation in a contaminated dredged sediment by mPIXE, mSXRF, EXAFS spectroscopy and principal component analysis. *Geochim. Cosmochim. Acta* **66,** 1549–1567.

Juillot F., Morin G., Ildefonse P., Trainor T. P., Benedetti M., Galoisy L., Calas G., and Brown G. E. (2003) Occurrence of Zn/Al hydrotalcite in smelter-impacted soils from northern France: Evidence from EXAFS spectroscopy and chemical extractions. *Am. Miner.* **88,** 509–526.

Krebs-Hartmann R. (1997) *In Situ Immobilization of Heavy Metals in Polluted Agricultural Soil—An Approach to Gentle Soil Remediation*. Ph.D. dissertation, Swiss Federal Institute of Technology, Zurich, Switzerland.

La Force M. J. and Fendorf S. (2000) Solid-phase iron characterization during common selective sequential extractions. *Soil Sci. Soc. Am. J.* **64,** 1608–1615.

Laperche V., Traina S. J., Gaddam P. G., and Logan T. J. (1996) Chemical and mineralogical characterization of Pb in a contaminated soil: Reactions with synthetic apatite. *Environ. Sci. Technol.* **30,** 3321–3326.

Lombi E., Hamon R. E., McGrath S. P., and McLaughlin M. J. (2003) Lability of Cd, Cu, and Zn in polluted soils treated with lime, beringite, and red mud and identification of a non-labile colloidal fraction of metals using isotopic techniques. *Environ. Sci. Technol.* **37,** 979–984.

Ma L. Q. (1996) Factors influencing the effectiveness and stability of aqueous lead immobilization by hydroxyapatite. *J. Environ. Qual.* **25,** 1420–1429.

Ma Q. Y., Traina S. J., Logan T. J., and Ryan J. A. (1993) *In situ* lead immobilization by apatite. *Environ. Sci. Technol.* **27,** 1803–1810.

Ma Q. Y., Logan T. J., and Traina S. J. (1995) Lead immobilization from aqueous solutions and contaminated soils using phosphate rocks. *Environ. Sci. Technol.* **29,** 1118–1126.

Malinowski E. R. (1978) Theory of error for target factor analysis with applications to mass spectrometry and nuclear magnetic resonance spectrometry. *Anal. Chim. Acta* **103,** 354–359.

Malinowski E. R. (1991) *Factor Analysis in Chemistry*. John Wiley, New York.

Manceau A., Boisset M. C., Sarret G., Hazemann R. L., Mench M., Cambier P., and Prost R. (1996) Direct determination of lead speciation in contaminated soils by EXAFS spectroscopy. *Environ. Sci. Technol.* **30,** 1540–1552.

Manceau A., Lanson B., Schlegel M., Hargé J. D., Musso M., Eybert-Bérard L., Hazemann J. L., Chateinger D., and Lamble G. M. (2000) Quantitative Zn speciation in smelter-contaminated soils by EXAFS spectroscopy. *Am. J. Sci.* **300,** 289–343.

Manceau A., Marcus M. A., and Tamura N. (2002) Quantitative speciation of heavy metals in soils and sediments by synchrotron X-ray techniques. In *Applications of Synchrotron Radiation in Low-Temperature Geochemistry and Environmental Science* (eds. N. C. Sturchio, P. Fenter, S. R. Sutton, and M. L. Rivers), *Rev. Mineral.* Mineralogical Society of America, Washington, DC.

Marcus M. A., MacDowell A. A., Celestre R., Manceau A., Miller T., Padmore H. A., and Sublett R. E. (2004) Beamline 10.3.2 at ALS: A hard X-ray microprobe for environmental and materials sciences. *J. Synch. Radiat.* **11,** 239–247.

McKenzie R. M. (1971) The synthesis of birnessite, cryptomelane, and some other oxides and hydroxide surfaces. *Z. Pflanzenernahr. Bodenk.* **150,** 99–102.

Mench M., Vangronsveld J., Didier V., and Clijsters H. (1994a) Evaluation of metal mobility, plant availability and immobilization by chemical agents in a limed-silty soil. *Environ. Pollut.* **86,** 279–286.

Mench M. J., Didier V. L., Löffler N., Gomez A., and Masson P. (1994b) A mimicked *in-situ* remediation study of metal-contaminated soil, with emphasis on cadmium and lead. *J. Environ. Qual.* **23,** 58–63.

Mench M., Vangronsveld J., Lepp N., and Edwards R. (1998) Physicochemical aspects and efficiency of trace element immobilization by soil amendments. In *Metal-Contaminated Soils: In-Situ Inactivation and Phytorestoration* (eds. J. Vangronsveld and S. Cunningham). Springer Verlag and Landes Bioscience.

Nachtegaal M. and Sparks D. L. (2003) Nickel sequestration in a kaolinite-humic acid complex. *Environ. Sci. Technol.* **37,** 529–534.

Nachtegaal M. and Sparks D. L. (2004) Effect of iron oxide coatings on zinc sorption mechanisms at the mineral/water interface. *J. Colloid Interface Sci.* **276,** 13–23.

Nies D. H., Nies A., and Chu L. (1989) Expression and nucleoleotide-sequence of a plasmid-determined divalent-cation efflux system from Alcaligenes-Eutrophus. *Proc. Natl. Acad. Sci. USA* **86,** 7351–7355.

Nriagu J. O. and Pacyna J. M. (1988) Quantitative assessment of worldwide contamination of air, water and soils by trace metals *Nature* **333,** 134–139.

O'Day P. A., Carroll S. A., and Waychunas G. A. (1998) Rock-water interactions controlling zinc, cadmium, and lead concentrations in surface waters and sediments, US Tri-State Mining District. 1: Molecular identification using X-ray absorption spectroscopy *Environ. Sci. Technol.* **32,** 943–955.

Oste L. A., Lexmond T. M.., and Van Riemsdijk W. H. (2002) Metal immobilization in soils using synthetic zeolites. *Environ. Qual.* **31,** 813–821.

Ostergren J. D., Brown G. E., Jr., Parks G. A., and Tingle T. N. (1999) Quantitative speciation of lead in selected mine tailings from Leadville, CO. *Environ. Sci. Technol.* **33,** 1627–1636.

Rebedea I. and Lepp N. (1994) The use of synthetic zeolites to reduce plant metal uptake and phytotoxicity in two polluted soils. *Sci. Tech. Lett.*, pp. 81-87.

Ressler T. (1997) WinXAS: A new software package not only for the analysis of energy-dispersive XAS data. *J. Physique IV* **7,** C2–C269.

Ressler T., Wong J., Roos J., and Smith I. L. (2002) Quantitative speciation of Mn-bearing particulates emitted from autos burning (mythylcyclopentadienyl)manganese tricarbonyl-added gasolines using XANES spectroscopy. *Environ. Sci. Technol.* **34,** 950–958.

Roberts D. R., Scheinost A. C., and Sparks D. L. (2002) Zinc speciation in a smelter-contaminated soil profile using bulk and microspectroscopic techniques. *Environ. Sci. Technol.* **36,** 1742–1750.

Roberts D. R., Nachtegaal M., and Sparks D. L. (2005) Speciation of metals in soils. In *Chemical Processes in Soils* (eds. M. A., Tabatai and D. L. Sparks). Soil Sci. Soc. Am., Madison, WI.

Scheidegger A. M., Lamble G. M., and Sparks D. L. (1997) Spectroscopic evidence for the formation of mixed-cation hydroxide phases upon metal sorption on clays and aluminum oxides. *J. Colloid Interface Sci.* **186,** 118–128.

Scheinost A. C., Kretzschmar R., and Pfister S. (2002) Combining selective sequential extractions, x-ray absorption spectroscopy, and principal component analysis for quantitative zinc speciation in soil. *Environ. Sci. Technol.* **36,** 5021–5028.

Schlegel M. L., Manceau A., Charlet L., and Hazemann J. L. (2001) Adsorption mechanisms of Zn on hectorite as a function of time, pH, and ionic strength. *Am. J. Sci.* **301,** 798–830.

Schwertmann U. and Cornell R. M. (1991) *Iron Oxides in the Laboratory: Preparation and Characterization*. Weinheim, New York.

Sobanska S., Ricq N., Laboudigue A., Guillermo R., Bremard C., Laureyns J., Merlin J. C., and Wignacourt J. P. (1999) Microchemical investigations of dust emitted by a lead smelter. *Environ. Sci. Technol.* **33,** 1334–1339.

Sonke J. E., Hoogewerff J. A., van der Laan S. R., and Vangronsveld J. (2002) A chemical and mineralogical reconstruction of Zn-smelter emissions in the Kempen region (Belgium), based on organic pool sediment cores. *Sci. Tot. Environ.* **292,** 101–119.

Sparks D. L. (1995) *Environmental Soil Chemistry*. Academic Press, Inc., London.

Strawn D. G. and Sparks D. L. (2000) Effects of soil organic matter on the kinetics and mechanisms of Pb(II) sorption and desorption in soil. *Soil Sci. Soc. Am. J.* **64,** 144–156.

Tessier A., Campbell P. G. C., and Bisson M. (1979) Sequential extraction procedure for the speciation of particulate trace metals. *Anal. Chem.* **51,** 844–851.

Tibazarwa C., Corbisier P., Mench M., Bossus A., Solda P., Mergeay M., Wyns L., and van der Lelie D. (2001) A microbial biosensor to predict bioavailable nickel in soil and its transfer to plants. *Environ. Pollut.* **113,** 19–26.

Trainor T. P., Brown G. E., Jr., and Parks G. A. (2000) Adsorption and precipitation of aqueous Zn(II) on alumina powders. *J. Colloid Interface Sci.* **231,** 359–372.

van der Lelie D., Schwuchow T., Schwidetzky U., Wuertz S., Baeyens W., Mergeay M., and Nies D. H. (1997) Two-component regulatory system involved in transcriptional control of heavy-metal homoeostasis in Alcaligenes eutrophus *Mol. Microbiol*. **23,** 493–503.

van der Lelie D., Verschaeve L., Regniers L., and Corbisier P. (1999) Use of bacterial tests (the VITOTOX genotoxicity test and the BIOMET heavy metal test) to analyze chemicals and environmental samples. In *Microbiotests for Routine Toxicity Testing and Biomonitoring* (ed. G. Persoone), pp. 197–208. Kluwer Academic/Plenum Publishers, Amsterdam, the Netherlands.

Vangronsveld J., Van Assche F., and Clijsters H. (1995) Reclamation of a bare industrial area contaminated by non-ferrous metals: *In situ* metal immobilization and fixation. *Environ. Pollut.* **87,** 51–59.

Vangronsveld J., Colpaert J. V., and Van Tichelen K. K. (1996) Reclamation of a bare industrial area contaminated by non-ferrous metals: Physico-chemical and biological evaluation of the durability of soil treatment and revegetation. *Environ. Pollut.* **94,** 131–140.

Vangronsveld J., Spelmans N., Clijsters H., Adriaensens E., Carleer R., Van Poucke L., van der Lelie D., Mergeay M., Corbisier P., Bierkens J., and Diels L. (2000) Physico-chemical and biological evaluation of the efficacy of in situ metal inactivation in contaminated soils. In *Proceedings of the 11th Annual International Conference on Heavy Metals in the Environment* (ed. J. Nriagu), contribution 1043. University of Michigan, School of Public Health, Ann Arbor, MI (CD-ROM).

Wasserman S. R., Allen P. G., Shuh D. K., Bucher J. J., and Edelstein N.M. (1999) EXAFS and principal component analysis: A new shell game. *J. Synchr. Radiat.* **6,** 284–286.

Waychunas G. A., Fuller C. C., and Davis J. A. (2002) Surface complexation and precipitate geometry for aqueous Zn(II) sorption on ferrihydrite I: X-ray absorption extended fine structure spectroscopy analysis. *Geochim. Cosmochim. Acta* **66,** 1119–1137.

Wickham G. A. (1990) Zinc industry in the 1990s. In *Lead-Zinc '90* (eds. T. S. Mackey and R. D. Prengaman), pp. 13–21. The Minerals, Metals and Materials Society, Warrendale, PA.

Zabinsky S. I., Rehr J. J., Ankudinov A., Albers R. C., and Eller M. J. (1995) Multiple-scattering calculations of X-ray absorption spectra. *Phys. Rev.* **B52**, 2995–3009.

Ziegler F., Scheidegger A. M., Johnson C. A., Dähn R., and Wieland E. (2001) Sorption mechanisms of zinc to calcium silicate hydrate: X-ray absorption fine structure (XAFS) investigation. *Environ. Sci. Technol.* **35,** 1550–1555.